

Enhanced U(VI) elimination from aqueous solution by FeS@biochar composites

Chengguang Chen^a, Zhenguo Shen^a, Muqing Qiu^{b,*}

^aSchool of Architectural Engineering, Shaoxing University Yuanpei College, Shaoxing 312000, China, emails: ccguang264@126.com (C. Chen), 16657403@qq.com (Z. Shen)

^bSchool of Life Science, Shaoxing University, Shaoxing 312000, China, email: qiumuqing@126.com (M. Qiu)

Received 24 April 2020; Accepted 10 September 2020

ABSTRACT

Iron sulfide nanoparticles were thought to be a potential material for U(VI) removal from aqueous solution. In order to overcome its aggregation and enhance removal capacity, biochar derived from peanut shell was chosen to support iron sulfide nanoparticles. The biochar supported iron sulfide nanoparticle composites (FeS@biochar) were prepared and applied for removal of U(VI) from aqueous solutions. The uptake capacity of U(VI) reached 59.52 mg/g at pH = 5.12 and 298 K, and it was indicated that the biochar supported with FeS significantly enhanced removal efficiency of U(VI). Based on scanning electron microscopy, X-ray diffraction, electronic differential system, Fourier transform infrared spectroscopy, and X-ray photoelectron spectroscopy analyses, it could be concluded that mechanism of removal of U(VI) ions by FeS@biochar was reductive reaction, electrostatic attraction and surface complexation. According to its high efficiency, reusability, and chemical stability, FeS@biochar can be considered in environmental remediation as a low cost and potential adsorbent for removal of U(VI) from aqueous solution.

Keywords: U(VI); Biochar; Iron sulfide nanoparticles

1. Introduction

The contamination of water body and groundwater because of the naturally occurring radioactive element (U(VI)) is a serious matter of concern [1]. The problem of radionuclide pollution from water body is becoming increasingly prominent [2,3]. In particular, wastewater containing U(VI) is thought as one of the most widespread pollution problems because of its radioactivity and toxicity to people [4,5]. The U(VI) pollution mainly comes from the production cycle of nuclear fuel [6,7]. In general, U(VI) mainly exists in the form of uranyl ions (UO₂²⁺) in aqueous solutions, which is not biodegradable. Additionally, it also accumulates in organisms, and may even harm human health [8,9]. Hence, a variety of methods, such as solvent extraction [10], chemical precipitation [11], flotation [12], membrane dialysis [13], and adsorption [14–16], have been tested and successfully applied into removal of uranium(VI)

from aqueous solutions. Among these treatment methods, adsorption method is the most commonly used method due to its simplicity, low cost and high efficiency [17]. Various types of adsorbents were applied in the treatment of wastewater, such as inorganic minerals [18], organic polymers [19], biomass [20], carbon-based materials [19], and composite materials [21]. Biochar is extensively thought as a green technology in response to removal of toxic contaminants in the solution such that they are not easily available to organisms. It also is a solid carbon-rich material produced from biomass residues [22], such as algae, animal manure, sewage sludge and crop straw. They are prepared through the following thermochemical processes, such as pyrolysis, torrefaction, hydrothermal carbonization and gasification. Furthermore, it is emerging as a cost-effective and environmentally friendly material for the adsorption of a variety of contaminants, such as antibiotics [23], agrochemicals [24], aromatic dyes [25], nutrients [26], heavy metals [27], and nuclides [28] from aqueous solution.

* Corresponding author.

However, the adsorption efficacy of biochar in contaminants is depended on its physicochemical structure. Therefore, in order to improve its adsorption performance, it is an urgent demand to develop cost effective, environmental friendly, and highly efficient sorbents for removal of toxic U(VI) from surface water [29].

Iron sulfide minerals are known to play an important role in reductive immobilization of U(VI) [30,31]. The nanoscale FeS can provide potentially greater reactivity, larger specific surface area, and soil deliverability [32]. Some researchers have illustrated that FeS nanoparticles showed high effectivity in treating various contaminants in water body and groundwater, such as radionuclides, chlorinated organic compounds, heavy metals, nitroaromatic compounds, oxyanions, and polychlorinated biphenyls [33]. However, the shortcoming of FeS nanoparticles is easy to be aggregated in solution. In order to overcome its aggregation and enhance removal capacity, more stabilized FeS nanoparticles have been tested [34].

In this research, biochar was chosen as stabilizer for FeS nanoparticles. FeS@biochar is prepared for adsorption experiment of U(VI) ions in solution. In this work, the main purpose was to explore the uptake capacity and removal mechanism of U(VI) ions by FeS@biochar. The objectives were: (1) preparation of FeS@biochar; (2) characterization of FeS@biochar; (3) experimentation of removal of U(VI) ions in solution by FeS@biochar; (4) exploration of removal mechanism of U(VI) by FeS@biochar.

2. Materials and methods

2.1. Materials

All chemical reagents in this experiment were of analytical grade. Ferrous sulfate heptahydrate ($\text{FeSO}_4 \cdot 7\text{H}_2\text{O}$), sodium sulfide nonahydrate ($\text{Na}_2\text{S} \cdot 9\text{H}_2\text{O}$), uranium nitrate hexahydrate ($\text{UO}_2\text{NO}_3 \cdot 6\text{H}_2\text{O}$; 99.99% purity), sodium hydroxide (NaOH) and hydrochloric acid (HCl) were purchased from Sinopharm Chemical Reagent Co., Ltd. (Shanghai, China). The peanut shell was obtained from a farm in Jinan City, Shangdong Province, China. Anaerobic deionized water was obtained by aerating N_2 into deionized water for over 30 min under the magnetic stirring condition. Then anaerobic deionized water was used in all experiments.

2.2. Preparation of adsorbents

The preparation of biochar and FeS nanoparticles was carried out according to the modified methods by Sun et al. [35]. The peanut shell was washed with deionized water for three times, and dried for 24 h at 110°C . The dried peanut shell was ground into 1–2 cm pieces and heated for 2 h at 250°C under nitrogen conditions. Then the black residues was pulverized and sieved through a 60 meshes sieve. Then, the biochar derived from peanut shell was obtained.

The iron sulfide nanoparticles (FeS) were synthesized according to the reaction of FeSO_4 with Na_2S . That is, 100 mL FeSO_4 solution (0.05 mol/L) was added into 250 mL Erlenmeyer flask containing 100 mL Na_2S solution (0.05 mol/L) and mixed for 30 min under continuous N_2 and magnetic stirring condition. Then suspensions were sealed and aged for

24 h to ensure the full growth of iron sulfide nanoparticles. Finally, the iron sulfide nanoparticles were obtained.

FeS@biochar was synthesized according to the modified methods by Lyu et al. [36]. According to this research, it was found that the composite material prepared by the mass ratio of iron sulfide nanoparticles and biochar to 1:4 had the best adsorption rate for U(VI). Therefore, the mass ratio of iron sulfide nanoparticles and biochar to 1:4 were used in this work. That was, 7.89 g of $\text{FeSO}_4 \cdot 7\text{H}_2\text{O}$ was added into 250 mL Erlenmeyer flasks containing 100 mL anaerobic deionized water under continuous N_2 and magnetic stirring condition. After 10 min, 10 g of biochar derived from peanut shell was added to the above FeSO_4 solution and magnetically stirred for 10 min again. Subsequently, 6.82 g of $\text{Na}_2\text{S} \cdot 9\text{H}_2\text{O}$ also was added to the above mixture and magnetic stirred for 20 min. The entire preparation process was under continuous N_2 and magnetic stirring condition. Then the suspension was sealed and aged for 24 h. The mixture was freeze-dried, washed with anaerobic deionized water for three times and freeze-dried again. The novel material of FeS@biochar was obtained.

2.3. Characterization of adsorbents

Scanning electron microscopy (SEM) (JEOL 6500F, Japan) was used to observe the surface morphology and structure of the adsorbent. The surface area and pore size of adsorbents were determined by the NOVA 4200e Surface area and Pore size analyzer (Quantachrome, FL, USA) at a relative pressure of 0.95 following the multipoint N_2 -BET adsorption method.

The surface functional groups of adsorbents in the wave number range of 500–4,000 cm^{-1} were recorded on a Nexus 670 FT-IR spectrometer (Thermo Nicolet, Madison). The crystalline structures of the adsorbents were conducted in a D/Max-III A Powder X-ray Diffractometer (XRD, Rigaku Corp., Japan). XPS (X-ray photoelectron spectrometer, Kratos AXIS Ultra DLD, Japan) and the model Axis-HS (Kratos Analytical) were used to determine surface adsorbents.

2.4. Adsorption experiments

All the adsorption experiments were carried out in 250 mL Erlenmeyer flasks at 200 rpm under a constant temperature condition. Typically, an amount of the adsorbent was added into a 250 mL Erlenmeyer flask containing 100 mL U(VI) initial concentration. Flask was sealed by bottle cap and placed in the shaker at 200 rpm and constant temperature. The anaerobic deionized water was used in all adsorption experiments. The pH was adjusted by 0.1 mol/L NaOH or HCl solutions. The entire adsorption process reached equilibrium and the supernatant was collected through filter filtration. The U(VI) concentration in the supernatant was analyzed by UV-Vis spectrophotometry [16]. The residual sample was centrifuged at 4,000 rpm for 5 min. Sediment was determined by microscopic technologies. All experiments were carried out in duplicate and the data were analyzed by the mean and standard deviation.

The removal rate ($R(\%)$) and the uptake capacity ($q(\text{mg/g})$) were calculated according to the following Eqs. (1) and (2).

$$R = \frac{C_0 - C_e}{C_0} \times 100\% \quad (1)$$

$$q = \frac{(C_0 - C_e) \times V}{m} \quad (2)$$

where C_0 (mg/L) and C_e (mg/L) were initial concentration and equilibrium concentration, respectively. V (L) was the solution volume and m (g) was the weight of the adsorbent.

In order to test the chemical stability of FeS@biochar, the reusable adsorption experiments were carried out for four times. 1.0 M Na_2CO_3 solution was chosen as desorbing solution.

3. Results and discussion

3.1. Characterization of FeS@biochar

Results show that the adsorption average pore width of biochar, FeS nanoparticles, and FeS@biochar are 3.94, 14.2, and 19.5 nm, respectively. BET specific surface areas of biochar, FeS nanoparticles, and FeS@biochar are 79.56, 5.32, and 48.3 m^2/g , respectively. The BET specific surface area of FeS@biochar was higher than that of FeS nanoparticles. This result indicated that FeS nanoparticles loaded on the biochar effectively prevent the aggregation of FeS nanoparticles. Because of biochar loading, the BET specific surface area of FeS@biochar was increased obviously. It indicated that FeS@biochar could be applied into the environmental treatment. The surface morphologies and microstructures of FeS@biochar composites were analyzed by SEM and electronic differential system (EDS) technologies.

As shown in Fig. 1a, it was depicted that the FeS nanoparticles were easy aggregative and had snow-like structure [37].

After FeS loaded on biochar, the FeS@biochar were uniformly dispersed (Fig. 1b). It was depicted that biochar highly improved the dispersibility of FeS nanoparticles. This was beneficial to decrease the aggregation of FeS nanoparticles in practical applications. The EDS spectrum and elemental mapping of FeS nanoparticles was detected by EDS analysis and shown in Figs. 1c and d. Four elements (C, O, S, and Fe) were uniformly observed on the surface of FeS@biochar. The weight proportions of C, O, S, and Fe were calculated to be 65.96%, 27.93%, 2.24%, and 3.88%, respectively. As shown in Fig. 2d, two major elements of FeS nanoparticles were observed on the surface of FeS@biochar. It depicted that biochar were supported successfully by FeS nanoparticles.

X-ray diffraction (XRD) patterns of biochar, FeS nanoparticles and FeS@biochar are shown in Fig. 2a. For biochar, a diffraction peak at 21.5° was ascribed to a layer-to-layer distance of 0.41 nm. The large d -spacing of the biochar was attributed to the presence of $-\text{OH}$, $\text{C}-\text{O}$, and $\text{O}=\text{C}-\text{O}$ functional groups [38].

For FeS nanoparticles, eight peaks at 29.9° , 33.6° , 35.4° , 43.1° , 47.1° , 53.1° , 60.3° , and 64.5° were observed. They were assigned to the indices (110), (004), (200), (110), (204), (205), (303), and (222) with planes (JCPDS No. 23–1120). Additionally, four peaks at 18.9° , 23.1° , 23.8° , and 26.5° also were observed. They were assigned to the characteristic peaks of Fe_3O_4 . The reason might be that a minor amount of FeS nanoparticles was oxidized by O_2 at atmosphere. The characteristic peaks of FeS and biochar both were observed on the surface of FeS@biochar. FeS nanoparticles and biochar were

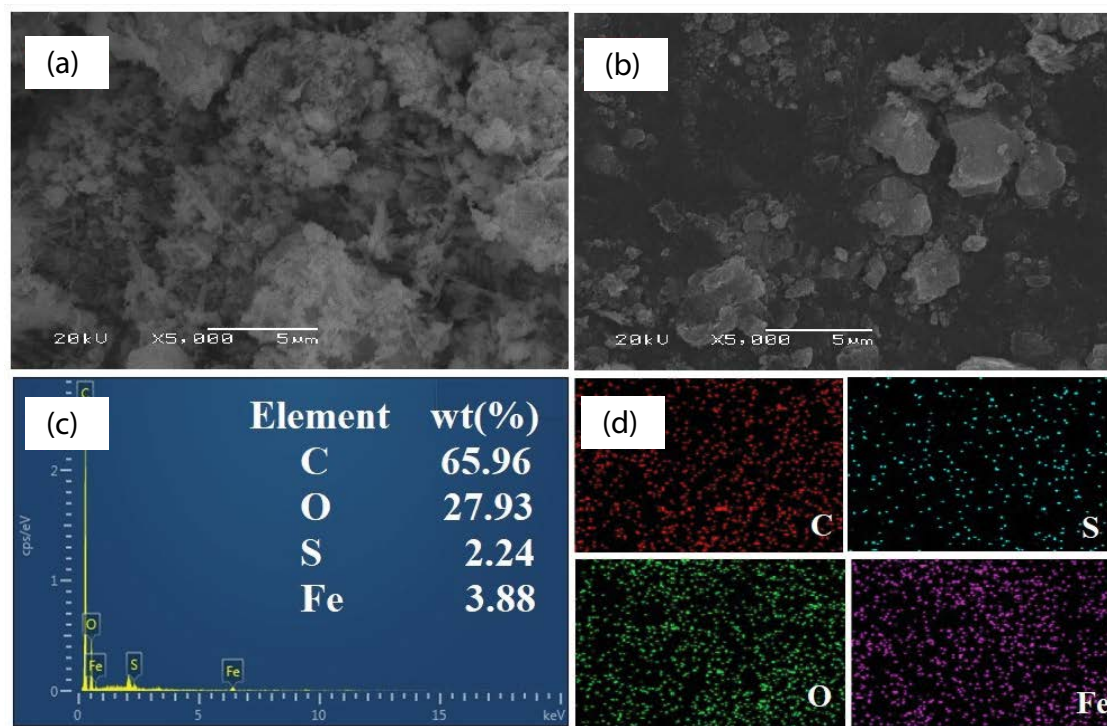


Fig. 1. SEM images of FeS nanoparticles (a) and FeS@biochar (b); EDS spectrum (c) and elemental mapping (d) of FeS nanoparticles.

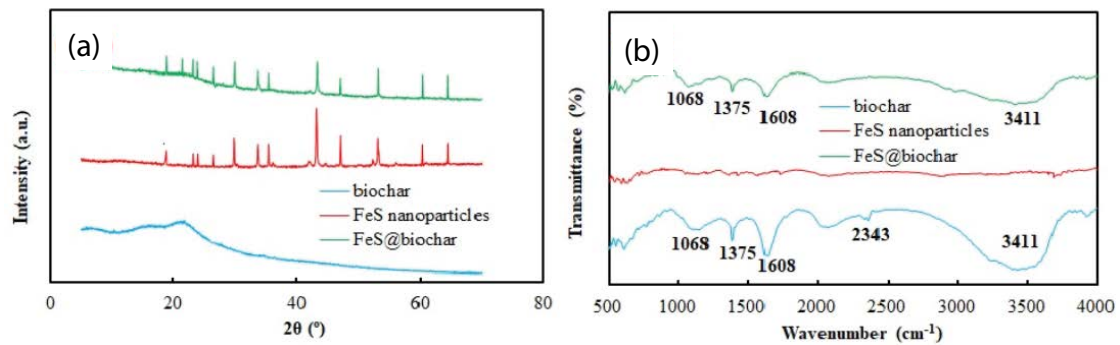


Fig. 2. XRD patterns (a) and FT-IR spectra (b) of biochar, FeS nanoparticles, and FeS@biochar.

present in the FeS@biochar composites. It indicated that FeS nanoparticles were supported successfully with biochar. The characteristic peaks of Fe_3O_4 also were found. It may be the reason that a small amount of Fe^{2+} ions were oxidized by O_2 at atmosphere during the preparation of FeS@biochar. Fourier transform infrared spectroscopy (FT-IR) spectra of biochar, FeS nanoparticles, and FeS@biochar are shown in Fig. 2b. For biochar, five characteristic peaks at 3,411; 2,343; 1,608; 1,375; and 1,068 cm^{-1} could be observed. They were ascribed to the vibrations of $-\text{OH}$, $-\text{CH}_2$, $\text{C}=\text{O}$, $\text{O}=\text{C}-\text{O}$, and alkoxy $\text{C}-\text{O}$ functional groups [39]. For FeS nanoparticles, characteristic peak was not observed. For FeS@biochar, four characteristic peaks for biochar could be observed. The characteristic peak at 2,343 cm^{-1} did not disappear on the spectra of surface of FeS@biochar. It should be this reason that molecular hydrogen bonding among FeS and biochar interacted [35].

Based on the above results of SEM, EDS, XRD, and FT-IR, it can be concluded that FeS@biochar in this work was obtained. The biochar derived from peanut shell was supported with FeS nanoparticles successfully. It not only had the properties of biochar from peanut shell but also had the properties of FeS nanoparticles.

3.2. Adsorption experiment

The effects of initial pH of solution, concentration of U(VI), reaction time, and temperature on removal rate were examined by adsorption experiment. Experimental results are shown in Fig. 3.

The initial pH in solution is a fundamental and important factor influencing element speciation, surface charge, and binding sites of adsorbent [40]. Removal of U(VI) by FeS@biochar was carried out with pH values ranging from

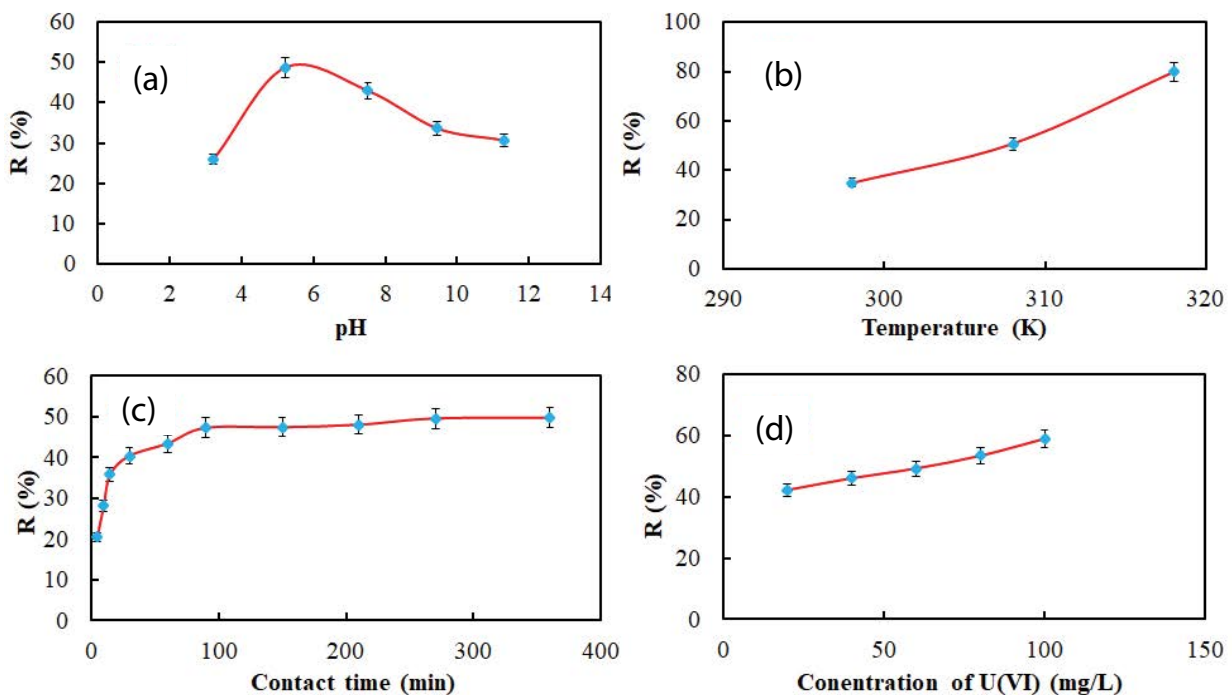


Fig. 3. Effect of initial pH (a), temperature (b), contact time (c), and concentration of U(VI) (d) on removal rate of U(VI) FeS@biochar. Experimental conditions: initial pH = 5.22, $C_0 = 60 \text{ mg/L}$, $m = 0.025 \text{ g}$, $V = 100 \text{ mL}$, $t = 360 \text{ min}$, and $T = 308 \text{ K}$.

2 to 12. As shown in Fig. 3a, the initial pH in solution had an important influence on the removal rate of U(VI). At first stage, the removal rate of U(VI) increased with the increasing pH in solution. While at pH above 6, the removal rate of U(VI) began to decrease with the increasing pH in solution. The species distribution of U(VI) ions using Visual MINTEQ (Version 3.0) at different pH is shown in Fig. 4.

It indicated that the species distribution of U(VI) ions in solution is mainly depended on pH value. In solution with pH less than 7, the main forms of U in aqueous solution were UO_2^{2+} , $(\text{UO}_2)_2(\text{OH})_2^{2+}$, and $\text{UO}_2(\text{OH})^+$. It also suggested that U was in the form of positively charged cations in aqueous solution. The concentration of UO_2^{2+} decreased with the increasing pH in solution. While the concentration of $(\text{UO}_2)_2(\text{OH})_2^{2+}$ and $\text{UO}_2(\text{OH})^+$ increased at first stage, then began to decrease slowly with the increasing pH in solution. In solution with pH above 7, the main forms of U in aqueous solution were $\text{UO}_2(\text{OH})_3^-$, $(\text{UO}_2)_3(\text{OH})_7^-$, and $\text{UO}_2(\text{OH})_4^{2-}$. It was also depicted that U was in the form of negatively charged cations in aqueous solution. When $\text{pH} < 7$, a large number of functional groups on the surface of FeS@biochar could adsorb positively charged cations through electrostatic attraction. However, the concentration of positively charged ionic groups of U(VI) increased at $\text{pH} > 7$. It was not beneficial to remove U(VI) by FeS@biochar at $\text{pH} > 7$. The removal rate of U(VI) decreased at $\text{pH} > 7$. At the same time, chemical precipitation reactions and ion exchange were also proceeding. Therefore, it could be thought that adsorption process, chemical precipitation process, and ion exchange process were important mechanisms on the removal of U(VI) by FeS@biochar when the initial pH was ranged from 2.0 to 12.0. The effect of temperature on the adsorption of U(VI) by FeS@biochar was also investigated (Fig. 3b). It displayed that the high temperature was beneficial for the removal rate of U(VI) ions by FeS@biochar. The removal rate of U(VI) increased with the increase of temperature. The removal rate reached 79.82% at 318 K.

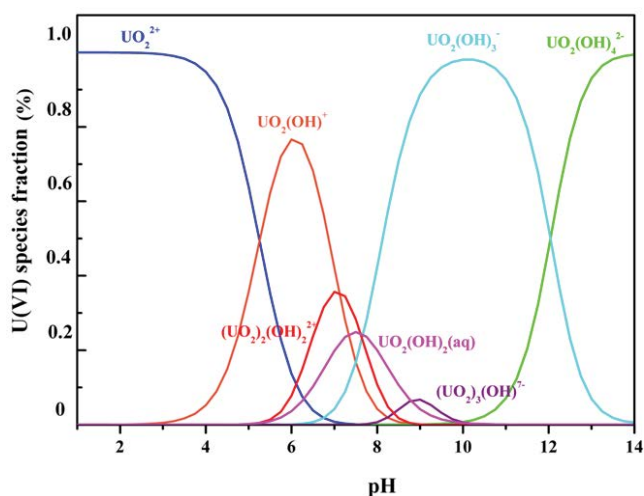


Fig. 4. Species distribution of U(VI) ions using Visual MINTEQ (Version 3.0). Experimental conditions: $C_0 = 60 \text{ mg/L}$, $V = 100 \text{ mL}$, $t = 360 \text{ min}$, $T = 308 \text{ K}$, and $m = 0.025 \text{ g}$.

The effect of reaction time on the adsorption of U(VI) by FeS@biochar was also tested (Fig. 3c). The removal rate increased very quickly at first stage of adsorption.

The removal rate reached 40.37% within 30 min. Then, the removal rate increased slowly, and it reached equilibrium at 360 min. At the first stage, the quick removal processes was attributed to the instantaneous electron transfer and surface complexation effects [41]. Then, the slow removal processes were attributed to the reducing efficiency of redox processes or the saturation of adsorption sites on external surface [42]. The concentration of U(VI) is an important factor affecting the mass transfer resistance of U(VI) between aqueous phases to solid phases. Experimental results are shown in Fig. 3d. The concentration of U(VI) was favorable for the removal of U(VI) by FeS@biochar. The removal rate of U(VI) increased when the concentration of U(VI) increased.

3.3. Effect of SO_4^{2-} ion in solution

The effect of SO_4^{2-} ion in solution on the removal of U(VI) by FeS@biochar is shown in Fig. 5.

From the figure, it can be concluded that the SO_4^{2-} ion in solution played an important role in the removal of U(VI) in aqueous solution. The removal rate of U(VI) by FeS@biochar decreased with the increase of SO_4^{2-} ions in solution. It might be attributed to the existence of Fe^{2+} ions on the surface of FeS@biochar. For adsorption sites, U(VI) ions are preferentially adsorbed over SO_4^{2-} ions in solution. When adsorption sites were saturated, the exchange reactions of dominate and competition for these sites between U(VI) ions and SO_4^{2-} ions were very important.

3.4. Adsorption kinetics, adsorption isotherm, and thermodynamics

To understand the adsorption process, adsorption kinetics, adsorption isotherm, and thermodynamics were discussed in details.

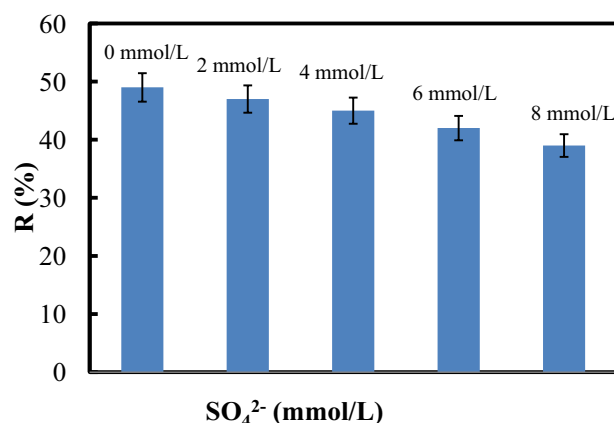


Fig. 5. Effect of SO_4^{2-} ion on the removal of U(VI) by FeS@biochar. Experimental conditions: initial $\text{pH} = 5.22$, $C_0 = 60 \text{ mg/L}$, $m = 0.025 \text{ g}$, $V = 100 \text{ mL}$, $t = 360 \text{ min}$, and $T = 308 \text{ K}$.

The equations of pseudo-first-order [43] and pseudo-second-order kinetic models [44] are described as Eqs. (3) and (4):

$$\ln(q_e - q_t) = \ln q_e - k_1 \times t \quad (3)$$

$$\frac{t}{q_t} = \frac{1}{(k_2 \times q_e^2)} + \frac{t}{q_e} \quad (4)$$

where q_e and q_t (mg/g) were the amount of U(VI) adsorbed at equilibrium and at time t , respectively. k_1 and k_2 are the pseudo-first-order and pseudo-second-order kinetic rate constants, respectively.

The Langmuir [45] and the Freundlich [46] equations are expressed by Eqs. (5) and (6):

$$\frac{C_e}{Q_e} = \frac{1}{Q_m \times K_L} + \frac{C_e}{Q_m} \quad (5)$$

$$Q_e = K_f \times C^n \quad (6)$$

where Q_e (mg/g) and C_e (mg/L) were the amount of adsorbed $^{238}\text{U(VI)}/^{241}\text{Am(III)}$ on AO/CNF and the equilibrium concentration in solution, respectively; Q_m (mg/g) was the maximum adsorption capacity; K_f ($\text{mg}^{1-n} \text{g}^{-1} \text{L}^n$) and n referred to an empirical constant related to adsorption capacity.

The thermodynamic parameters (i.e., the standard Gibbs free energy change $-\Delta G^\circ$, the standard enthalpy

change $-\Delta H^\circ$, the standard entropy change $-\Delta S^\circ$) were calculated by Eqs. (7) and (8):

$$\Delta G^\circ = -RT \ln K^\circ \quad (7)$$

$$\ln K^\circ = \frac{\Delta S^\circ}{R} - \frac{\Delta H^\circ}{(RT)} \quad (8)$$

where R and T were universal gas constant (8.314 J/(mol K)) and temperature (K), respectively. K° was adsorption equilibrium constants, which could be calculated by plotting $\ln K_q$ vs. C_e and extrapolating C_e to zero.

According to experimental data of Fig. 3c, the fitting curves of pseudo-first-order kinetic and pseudo-second-order kinetic models are displayed in Figs. 6a and b.

The value of R^2 could be calculated. It indicated that the adsorption process could be ascribed by pseudo-second-order kinetic model because of higher value of R^2 (0.9958 > 0.9061). It also demonstrated that the adsorption process involved in the removal of U(VI) was chemical reaction [47]. Figs. 6c and d show the fitting curves of Langmuir isotherm model and Freundlich isotherm model. The adsorption process of U(VI) by FeS@biochar followed Langmuir isotherm model on the basis of the good correlation coefficient parameter of R^2 . It suggested that the adsorption process mainly was monolayer reaction process. The maximum uptake capacity of U(VI) by FeS@biochar could be calculated to be 59.52 mg/g according to the Langmuir isotherm model. Compared with the reported adsorbents [48], FeS@biochar show higher

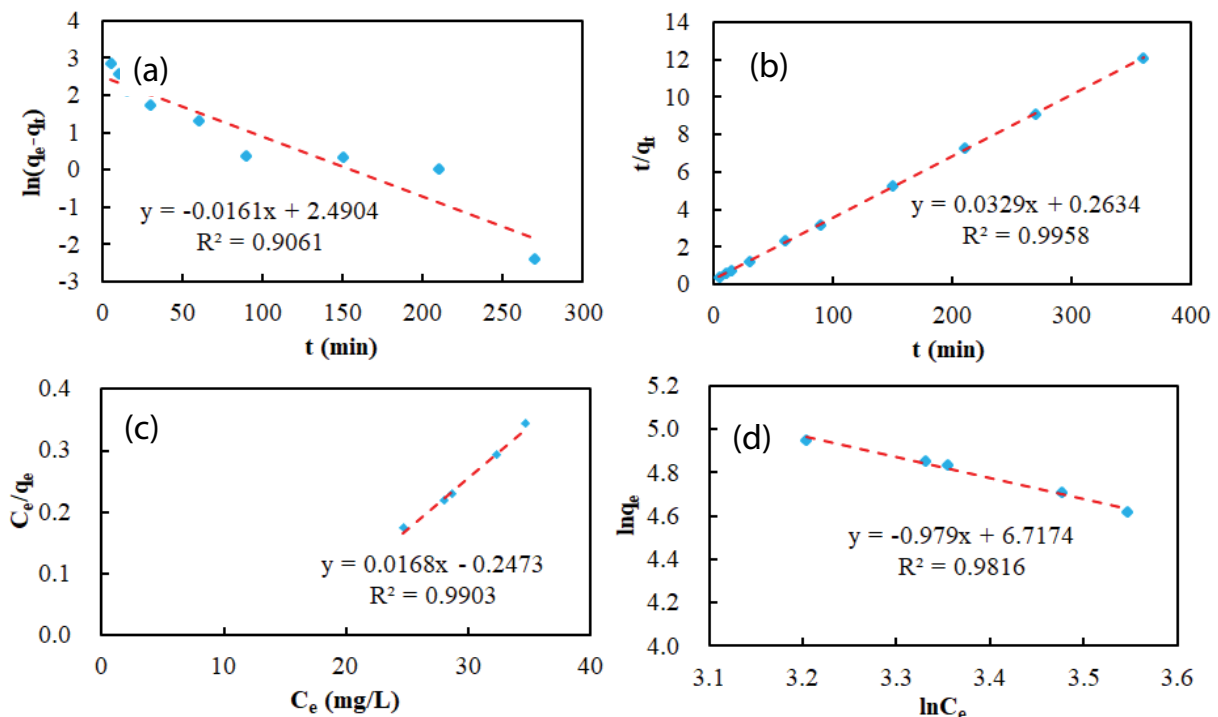


Fig. 6. Adsorption kinetic of U(VI) ions and adsorption isotherm of U(VI) ions by FeS@biochar (a) pseudo first-order kinetic model, (b) pseudo second-order kinetic model, (c) Langmuir, and (d) Freundlich. Experimental conditions: $t = 360$ min, $C_0 = 60$ mg/L, $V = 100$ mL, $\text{pH} = 5.22$, $T = 308$ K, and $m = 0.025$ g.

removal rate of U(VI). It indicated the biochar supported with FeS significantly enhanced removal efficiency of U(VI).

The thermodynamic feasibility study was also an important parameter for describing the adsorption processes. Therefore, the thermodynamic parameters are tabulated in Table 1.

The negative ΔG° indicated that the removal of U(VI) was a spontaneous reaction. While, the positive ΔS° demonstrated that the removal process was disordering the systems. Additionally, the positive ΔH° suggested that the removal process was an endothermic reaction. Therefore, higher temperature could enhance dehydration. In a word, it could be concluded that removal of U(VI) by FeS@biochar was a spontaneous and endothermic process.

3.5. Adsorption mechanism

To further explore the adsorption mechanism, the higher technology analytical method X-ray photoelectron spectroscopy (XPS) was adopted. The results of XPS analyses before and after reaction with U(VI) are displayed in Fig. 7.

As shown in Fig. 7a, four photoelectron lines at binding energies of ~167, ~286, ~533, and ~731 eV were observed for FeS@biochar before reaction with U(VI). They were related to S 2p, C 1s, O 1s, and Fe 2p, respectively. It also indicated that the primary elements for FeS@biochar were S, Fe, C, and O. The results were consistent with the results

of EDS (Fig. 1c). After adsorption of U(VI), these photoelectron lines also could be observed. Moreover, the two new peaks at ~382 and ~393 eV were appeared. They were attributed to U 4f_{7/2} and U 4f_{5/2}. It could be concluded that FeS@biochar could interact with U(VI) ion from aqueous solution. From Fig. 7b, it could be converted into four peaks at ~381.82, ~382.51, ~392.52, and ~392.53 eV. They were ascribed to U(VI) and U(IV), respectively [49]. It indicated that part of U(VI) was adsorbed by the functional group on the surface of FeS@biochar and part of U(VI) was reduced to U(IV) by FeS.

In a word, the proposed removal mechanism could be suggested that U(VI) ions were removed through reductive reaction, electrostatic attraction, and surface complexation (Fig. 8). The biochar not only prevented FeS nanoparticles from being aggregated but also enhanced removal capacity of U(VI) ions. The functional groups on the FeS@

Table 1
Thermodynamic parameters for U(VI) removal on FeS@biochar

Temperature	ΔG° (kJ/mol)	ΔH° (kJ/mol)	ΔS° (J/(mol K))
298 K	-1.89		
318 K	-3.63	78.46	268.62
338 K	-7.3		

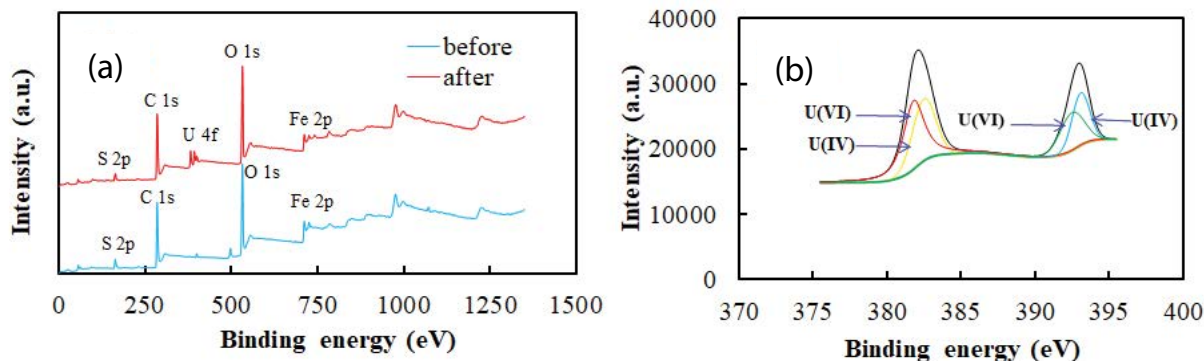


Fig. 7. XPS survey spectra of FeS@biochar before and after reaction with U(VI) (a) and XPS spectrum of U(IV) (b).

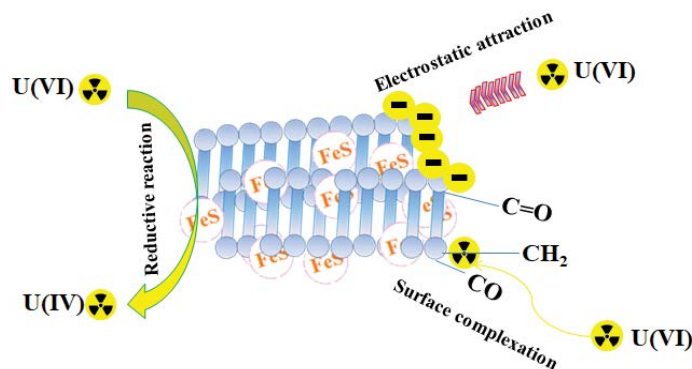


Fig. 8. Proposed removal mechanism of U(VI) by FeS@biochar.

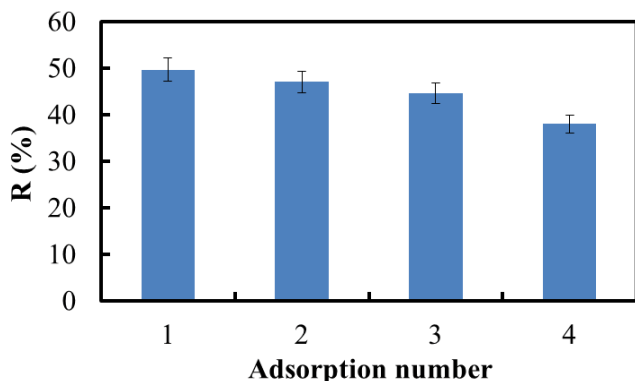


Fig. 9. Removal rate of U(VI) by FeS@biochar under a different adsorption number. Experimental conditions: $t = 360$ min, $C_0 = 60$ mg/L, $V = 100$ mL, $pH = 5.22$, $T = 308$ K, and $m = 0.025$ g.

biochar could react with U(VI) ions through electrostatic attraction and surface complexation. Additionally, FeS nanoparticles could remove U(VI) by redox reactions.

3.6. Chemical stability of FeS@biochar

The results of chemical stability of FeS@biochar are shown in Fig. 9. The removal rate decreased with the increase of adsorption number. The removal rate reached 49.62% at first time. The removal rate still could reach 38.16% after four times of reuse. It could be concluded that the preparation of FeS@biochar in this work was reusability and chemical stability material.

4. Conclusions

The biochar supported iron sulfide nanoparticle composites was prepared and applied for removal of U(VI) from aqueous solution. Based on the results of SEM, EDS, XRD, and FT-IR, the iron sulfide nanoparticles successfully were loaded on the biochar. A number of functional groups were observed on the surface of FeS@biochar. The operational parameters had an important effect on the removal of U(VI) from aqueous solution. The adsorption process of U(VI) by FeS@biochar followed pseudo-second-order kinetic model and Langmuir isotherm model. Removal of U(VI) by FeS@biochar was a spontaneous and endothermic processes. Additionally, the mechanism of removal of U(VI) mainly was adsorption and reductive process. The FeS@biochar was a reusable and chemically stable material.

Acknowledgments

This work is financially supported by the Natural Science Foundation of Zhejiang Province, China (No. LGF20C030001) and College Student Innovation and Entrepreneurship Training Program, China (No. 201910349007). The authors are very grateful for the support.

References

[1] S. Kumar, V.A. Loganathan, R.B. Gupta, M.O. Barnett, An assessment of U(VI) removal from groundwater using biochar

produced from hydrothermal carbonization, *J. Environ. Manage.*, 92 (2011) 2504–2512.

[2] L. Dolatyari, M.R. Yaftian, S. Rostamnia, M.S. Seyeddoraji, Multi-variate optimization of a functionalized SBA-15 mesoporous based solid-phase extraction for U(VI) determination in water samples, *Anal. Sci.*, 33 (2017) 769–776.

[3] N. Li, M.L. Yin, D.C.W. Tsang, S.T. Yang, J. Liu, X. Li, G. Song, J. Wang, Mechanisms of U(VI) removal by biochar derived from *Ficus microcarpa* aerial root: a comparison between raw and modified biochar, *Sci. Total Environ.*, 697 (2019) 134115–134126.

[4] Y. Liu, X. Liu, W. Dong, L. Zhang, Q. Kong, W. Wang, Efficient adsorption of sulfamethazine onto modified activated carbon: a plausible adsorption mechanism, *Sci. Rep.*, 7 (2017) 12437–12445.

[5] Z. Dousti, L. Dolatyari, M.R. Yaftian, S. Rostamnia, Adsorption of Eu(III), Th(IV), and U(VI) by mesoporous solid materials bearing sulfonic acid and sulfamic acid functionalities, *Sep. Sci. Technol.*, 54 (2019) 2606–2624.

[6] J. Liu, X. Luo, J. Wang, T. Xiao, M. Yin, N.S. Belshaw, H. Lippold, L. Kong, E. Xiao, Z. Bao, N. Li, Y. Chen, W. Linghu, Provenance of uranium in a sediment core from a natural reservoir, South China: application of Pb stable isotope analysis, *Chemosphere*, 193 (2018) 1172–1180.

[7] L. Zhang, Y. Li, H. Guo, H. Zhang, N. Zhang, T. Hayat, Y. Sun, Decontamination of U(VI) on graphene oxide/ Al_2O_3 composites investigated by XRD, FT-IR and XPS techniques, *Environ. Pollut.*, 248 (2019) 332–338.

[8] R. Krachler, R. Krachler, F. Gülce, B.K. Keppler, G. Wallner, Uranium concentrations in sediment pore waters of Lake Neusiedl, Austria, *Sci. Total Environ.*, 633 (2018) 981–988.

[9] L. Dolatyari, M. Shateri, M.R. Yaftian, S. Rostamnia, Unmodified SBA-15 adsorbents for the removal and separation of Th(IV) and U(VI) ions: the role of pore channels and surface-active sites, *Sep. Sci. Technol.*, 54 (2019) 2863–2878.

[10] H. Singh, S.L. Mishra, R. Vijayalakshmi, Uranium recovery from phosphoric acid by solvent extraction using a synergistic mixture of di-nonylphenyl phosphoric acid and tri-n-butyl phosphate, *Hydrometallurgy*, 73 (2004) 63–70.

[11] A. Mellah, S. Chegrouche, M. Barkat, The precipitation of ammonium uranyl carbonate (AUC): thermodynamic and kinetic investigations, *Hydrometallurgy*, 85 (2007) 163–171.

[12] T.P. Rao, P. Metilda, J.M. Gladis, Preconcentration techniques for uranium(VI) and thorium(IV) prior to analytical determination—an overview, *Talanta*, 68 (2006) 1047–1064.

[13] H. Omar, H. Arida, A. Daifullah, Adsorption of ^{60}Co radionuclides from aqueous solution by raw and modified bentonite, *Appl. Clay Sci.*, 44 (2009) 21–26.

[14] A.J. Fuller, S. Shaw, C.L. Peacock, D. Trivedi, I.T. Burke, EXAFS study of Sr sorption to illite, goethite, chlorite, and mixed sediment under hyperalkaline conditions, *Langmuir*, 32 (2016) 2937–2946.

[15] S.P. Boeykens, M.N. Piol, L. SamudioLegal, A.B. Saralegui, C. Vazquez, Eutrophication decrease: phosphate adsorption processes in presence of nitrates, *J. Environ. Manage.*, 203 (2017) 888–895.

[16] M.X. Li, H.B. Liu, T.H. Chen, C. Dong, Y.B. Sun, Synthesis of magnetic biochar composites for enhanced uranium (VI) adsorption, *Sci. Total Environ.*, 651 (2019) 1020–1028.

[17] L. Li, M. Yang, Q. Lu, W.K. Zhu, H.Q. Ma, L.C. Dai, Oxygen-rich biochar from torrefaction: a versatile adsorbent for water pollution control, *Bioresour. Technol.*, 294 (2019) 122142–122153.

[18] H.E. Roberts, K. Morris, G.T.W. Law, J.F.W. Mosselmans, P. Bots, K. Kvashnina, S. Shaw, Uranium(V) incorporation mechanisms and stability in Fe(II)/Fe(III) (oxyhydr) oxides, *Environ. Sci. Technol. Lett.*, 4 (2017) 421–426.

[19] M.B. Ahmed, J.L. Zhou, H.H. Ngo, W. Guo, M. Chen, Progress in the preparation and application of modified biochar for improved contaminant removal from water and wastewater, *Bioresour. Technol.*, 214 (2016) 836–851.

[20] V.S. Tran, H.H. Ngo, W. Guo, J. Zhang, S. Liang, C. Ton-That, X. Zhang, Typical low cost biosorbents for adsorptive removal

- of specific organic pollutants from water, *Bioresour. Technol.*, 182 (2015) 353–363.
- [21] L. Dolatyari, M.R. Yaftian, S. Rostamnia, Adsorption of Th(IV) and U(VI) on functionalized SBA-15 mesoporous silica materials using fixed bed column method: breakthrough curves prediction and modeling, *Sep. Sci. Technol.*, 53 (2018) 1282–1294.
- [22] Y.L. Lu, S. Song, R.S. Wang, Z.Y. Liu, J. Meng, A.J. Sweetman, A. Jenkins, R.C. Ferrier, H. Li, W. Luo, T.Y. Wang, Impacts of soil and water pollution on food safety and health risks in China, *Environ. Int.*, 77 (2015) 5–15.
- [23] H. Liu, Y.F. Wei, J.M. Luo, T. Li, D. Wang, S.L. Luo, J.C. Crittenden, 3D hierarchical porous structured biochar aerogel for rapid and efficient phenicol antibiotics removal from water, *Chem. Eng. J.*, 368 (2019) 639–648.
- [24] F. Xiao, J.J. Pignatello, Effects of post-pyrolysis air oxidation of biomass chars on adsorption of neutral and ionizable compounds, *Environ. Sci. Technol.*, 50 (2016) 6276–6283.
- [25] L. Dai, W. Zhu, L. He, F. Tan, N. Zhu, Q. Zhou, M. He, G. Hu, Calcium-rich biochar from crab shell: an unexpected super adsorbent for dye removal, *Bioresour. Technol.*, 267 (2018) 510–516.
- [26] L. Dai, F. Tan, H. Li, N. Zhu, M. He, Q. Zhu, G. Hu, L. Wang, J. Zhao, Calcium rich biochar from the pyrolysis of crab shell for phosphorus removal, *J. Environ. Manage.*, 198 (2017) 70–74.
- [27] H. Hao, Y.D. Jing, W.L. Ju, L. Shen, Y.Q. Cao, Different types of biochar: effect of aging on the Cu(II) adsorption behavior, *Desal. Water Treat.*, 95 (2017) 227–233.
- [28] L. Dolatyari, M.R. Yaftian, S. Rostamnia, Removal of uranium(VI) ions from aqueous solutions using schiff base functionalized SBA-15 mesoporous silica materials, *J. Environ. Manage.*, 169 (2016) 8–17.
- [29] L. Wang, H. Song, L. Yuan, Z. Li, Y. Zhang, J. Gibson, L. Zheng, Z. Chai, W. Shi, Efficient U(VI) reduction and sequestration by Ti₂C₁₂MXene, *Environ. Sci. Technol.*, 52 (2018) 10748–10756.
- [30] N.F. Spycher, M. Issarangkun, B.D. Stewart, S. Sevinc, E.B. Şengör, T.R. Ginn, B.M. Peyton, R.K. Sani, Biogenic uraninite precipitation and its reoxidation by iron(III) (hydr) oxides: a reaction modeling approach, *Geochim. Cosmochim. Acta*, 75 (2011) 4426–4440.
- [31] H. Veeramani, A.C. Scheinost, N. Monsegue, N.P. Qafoku, R. Kukkadapu, M. Newville, A. Lanzirrotti, A. Pruden, M. Murayama, M.F. Hochella, Abiotic reductive immobilization of U(VI) by biogenic mackinawite, *Environ. Sci. Technol.*, 47 (2013) 2361–2369.
- [32] D. Shao, X. Ren, J. Wen, S. Hu, J. Xiong, T. Jiang, X. Wang, X. Wang, Immobilization of uranium by biomaterial stabilized FeS nanoparticles: effects of stabilizer and enrichment mechanism, *J. Hazard. Mater.*, 302 (2016) 1–9.
- [33] Y. Gong, J. Tang, D. Zhao, Application of iron sulfide particles for groundwater and soil remediation: a review, *Water Res.*, 89 (2016) 309–320.
- [34] Y. Gong, Y. Liu, Z. Xiong, D. Zhao, Immobilization of mercury by carboxymethyl cellulose stabilized iron sulfide nanoparticles: reaction mechanisms and effects of stabilizer and water chemistry, *Environ. Sci. Technol.*, 48 (2014) 3986–3994.
- [35] Y. Sun, Z.M. Lou, J.B. Yu, X.X. Zhou, D. Lv, J.S. Zhou, S.A. Baig, X.H. Xu, Immobilization of mercury(II) from aqueous solution using Al₂O₃-supported nanoscale FeS, *Chem. Eng. J.*, 323 (2017) 483–491.
- [36] H. Lyu, J.C. Tang, Y. Huang, L.S. Gai, E.Y. Zeng, K. Liber, Y.Y. Gong, Removal of hexavalent chromium from aqueous solutions by a novel biochar supported nanoscale iron sulfide composite, *Chem. Eng. J.*, 322 (2017) 516–524.
- [37] S. Bae, R. Collins, T. Waite, K. Hanna, Advances in surface passivation of nanoscale zero valent iron: a critical review, *Environ. Sci. Technol.*, 52 (2018) 12010–12025.
- [38] M.Y. Yen, C.C. Ten'g, M.C. Hsiao, P.I. Liu, W.P. Chuang, C.C.M. Ma, C.K. Hsieh, M.C. Tsai, C.H. Tsai, Platinum nanoparticles/graphene composite catalyst as a novel composite counter electrode for high performance dyesensitized solar cells, *J. Mater. Chem.*, 21 (2011) 12880–12892.
- [39] H. Lyu, Y. Gong, J. Tang, Y. Huang, Q. Wang, Immobilization of heavy metals in electroplating sludge by biochar and iron sulfide, *Environ. Sci. Pollut. Res. Int.*, 36 (2016) 1–17.
- [40] Y.H. Wu, H.W. Pang, Y. Liu, X.X. Wang, S.J. Yu, D. Fu, J.R. Chen, X.K. Wang, Environmental remediation of heavy metal ions by novel-nanomaterials: a review, *Environ. Pollut.*, 246 (2019) 608–620.
- [41] J. Lan, Z. Chai, W. Shi, A combined DFT and molecular dynamics study of U(VI)/calcite interaction in aqueous solution, *Sci. Bull.*, 62 (2017) 1064–1073.
- [42] P. Gu, S. Zhang, X. Li, X. Wang, T. Wen, R. Jehan, A. Alsaedi, T. Hayat, X. Wang, Recent advances in layered double hydroxide-based nanomaterials for the removal of radionuclides from aqueous solution, *Environ. Pollut.*, 240 (2018) 493–505.
- [43] S. Lagergren, Zur theorie der sogenannten adsorption gelöster stoffe, *K. Sven. Vetenskapsakad. Handl.*, 24 (1898) 1–39.
- [44] Y.S. Ho, G. McKay, Pseudo-second order model for sorption processes, *Proc. Biochem.*, 34 (1999) 451–465.
- [45] I. Langmuir, The adsorption of gases on plane surface of glass, mica and platinum, *J. Am. Chem. Soc.*, 40 (1918) 1361–1403.
- [46] H.M.F. Freundlich, Über die adsorption in lasungen, *J. Phys. Chem.*, 57 (1906) 385–470.
- [47] C. Zhang, Y. Liu, X. Li, H. Chen, T. Wen, Z. Jiang, Y. Ai, Y. Sun, T. Hayat, X. Wang, Highly uranium elimination by crab shells-derived porous graphitic carbon nitride: batch, EXAFS and theoretical calculations, *Chem. Eng. J.*, 346 (2018) 406–415.
- [48] Q. Hu, Y. Zhu, B. Hu, S. Lu, G. Sheng, Mechanistic insights into sequestration of U(VI) toward magnetic biochar: batch, XPS and EXAFS techniques, *J. Environ. Sci.*, 70 (2018) 217–225.
- [49] H. Guo, H.H. Wang, N. Zhang, J.X. Li, J. Liu, A. Alsaedi, T. Hayat, Y. Li, Y.B. Sun, Modeling and EXAFS investigation of U(VI) sequestration on Fe₃O₄/PCMs composites, *Chem. Eng. J.*, 369 (2019) 736–744.